# Insights and Criteria for an Efficient and Accurate Calculation of Self- and Cross-Heating Transients

Oleksandr Kyryliv* and Luca Selmi*
*Department of Engineering "Enzo Ferrari", University of Modena and Reggio Emilia, Modena, Italy
Email: oleksandr.kyryliv@unimore.it, luca.selmi@unimore.it

***Abstract*—Starting from the generalized expression of the complex thermal impedance of uniform slabs, this paper derives a strategy to define analytical expressions with controlled complexity and accuracy for the space/time-dependent overtemperature induced by an ideal step power source. These expressions, possibly but not necessarily translated into Foster-type lumped element networks, support the efficient and robust extraction of physically meaningful thermal conductivity and specific heat values via optimized fitting to thermal transients' data. The results are also useful to predict the temperature rise/fall time at a given distance from the power source; hence, to interpret transient self-heating and cross-heating in electronic devices.**

***Index Terms*—Thermal modelling, Self-heating, Cross-heating.**

## I. Introduction

Device self-heating (SH), cross-heating (CH) and overtemperature ($\Delta T$=$T$-$T_{amb}$) are attracting increasing attention in modern nanoelectronics, where vertical transistor architectures (FinFET, NSFET, CFET) and 3D (heterogeneous) integration at the chip, wafer and package level are widely spreading out [1], [2]. In these tightly confined architectures with multiple heat sources, structural thermal isolation significantly hinders heat dissipation, degrading carrier mobility and accelerating critical failure mechanisms [3], [4]. Accurate and efficient thermal and coupled electro-thermal modeling is thus needed from device to system level. Simulations by Technology Computer-Aided Design (TCAD) address most needs at the former level. However, analytical and lumped-element descriptions are also needed and challenging, because translating heat diffusion into compact models with physically meaningful parameters poses constraints on the equivalent thermal circuits' topology and the transcendental expressions of the lumped elements [5], [6].

In this work, we study and compare three general, exact, and equivalent but distinct expressions for the space/time-dependent overtemperature, $\Delta T(z,t)$, at position $z$ between a step heat source and a room temperature boundary, in a uniform semiconductor slab, Fig.1. We then develop: 1) an exact formula for the $z$-dependent temperature rise time to 97% of its steady state value; 2) quantitative criteria to minimize the expressions' complexity with controlled accuracy in a given time interval; 3) a least-complexity, piecewise solution for the whole transient. Finally, we discuss strategies to best use the results for the extraction of accurate physical thermal parameters from measured temperature transients following an abrupt heating.

## II. Analytical Derivations and Model Equations

The derivation starts with the linear heat equation in a 1D domain (Fig. 1) where the thermal conductivity ($\kappa$) and volumetric heat capacity ($c_v$) are uniform in space and constant in temperature. Small deviations from linearity can be dealt with the Kirchhoff transformation [7]. We impose mixed Neumann/Dirichlet boundary conditions $q(t) = P(t)/A_0$ at $z = 0$ and $\Delta T = T - T_{amb} = 0$ at $z = z_0$, respectively, where $P(t)$ [W] is the power waveform and $A_0$ the injection area.

$$c_v \frac{\partial \Delta T}{\partial t} = \kappa \frac{\partial^2 \Delta T}{\partial z^2} \quad (1)$$

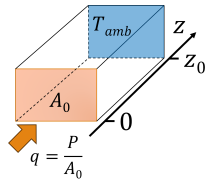


Fig. 1. Heat conduction equation and sketch of the reference structure, key variables, and boundary conditions.

Upon Laplace transformation in time and the solution of the differential equation in $z$, the thermal impedance at $z$, i.e., the response to a Dirac's delta power impulse at $z = 0$, is:

$$Z_{th}(z,s) = \frac{\Delta T(z,s)}{P(s)} = \frac{1}{A_0\sqrt{c_v \kappa s}} \frac{\sinh\left((z_0 - z)\sqrt{s/\alpha}\right)}{\cosh\left(z_0\sqrt{s/\alpha}\right)} \quad . \tag{2}$$

Note that for $z = 0$, Eq. 2 yields the well-known result for a short-circuited RC transmission line [8], [9].

The overtemperature waveform following the step power excitation $P(s) = P/s$ is readily obtained by inverse Laplace transformation of $\Delta T(z,s) = PZ_{th}(z,s)/s$ and yields [10]:

$$\begin{aligned} \Delta T(z,t) = \frac{P}{A_0\sqrt{\kappa c_v}} \sum_{m=0}^{\infty} (-1)^m \times \\ \times \Bigg[ + 2\sqrt{\frac{t}{\pi}} \exp\left(-\frac{d_-^2}{4\alpha t}\right) - \frac{d_-}{\sqrt{\alpha}} \operatorname{erfc}\left(\frac{d_-}{2\sqrt{\alpha t}}\right) \\ -2\sqrt{\frac{t}{\pi}} \exp\left(-\frac{d_+^2}{4\alpha t}\right) + \frac{d_+}{\sqrt{\alpha}} \operatorname{erfc}\left(\frac{d_+}{2\sqrt{\alpha t}}\right) \Bigg] \end{aligned} \tag{3}$$

where $\alpha = \kappa/c_v$ is the thermal diffusivity and the auxiliary variables $d_+ = [2(m+1)z_0 - z]$, $d_- = [2mz_0 + z]$ encapsulate the spatial dependence. Fig. 2 confirms the correctness of Eq. 3 by comparison with finite element TCAD solutions of Eq. 1 with Raphael [11].

979-8-3195-0631-3/26/$31.00 ©2026 IEEE

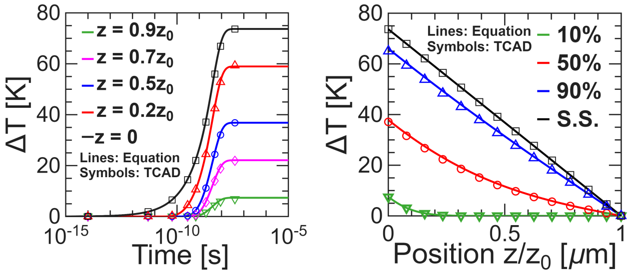


Fig. 2. TCAD simulations (symbols) and $\Delta T$ model (Eq.3, lines) in the time (left) and space (right) domains, for different positions and times of percentage completion of the transient, respectively. S.S. means steady state. $z_0 = 1\,\mu$m, $A_0 = 0.08\,\mu\text{m}^2$, $\kappa = 1.69\,$W/K cm, $c_v = 1.63\,$W/K cm$^3$ as in silicon.

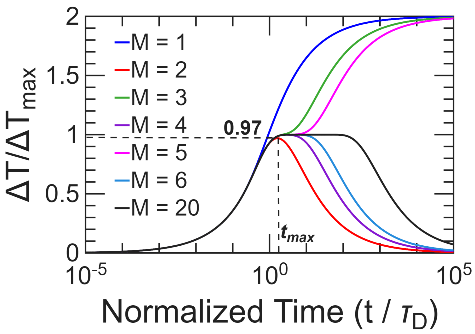


Fig. 3. Normalized $\Delta T(0,t)$ adding the terms with $m \in [0, M\text{-}1]$ in Eq. 3.

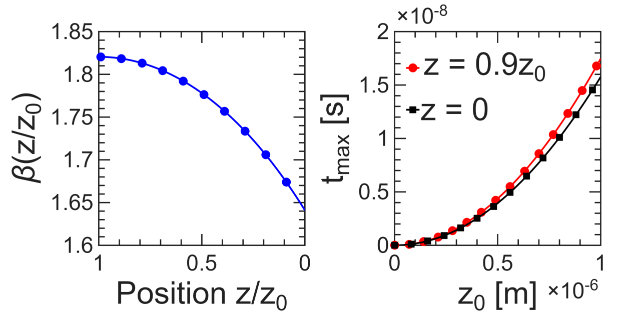


Fig. 4. : Left: $\beta$ as a function of $z/z_0$; Right: $t_{max}(z)$ vs $z_0$ computed for $M = 2$ and two $z$ values. Parameters as in Fig. 2. $\tau_D = c_v z_0^2/\kappa = 9.61$ ns.

Eq. 3 comprises an infinite series of Gaussian and complementary error functions with alternating signs, corresponding to spatially offset images of the power source, enforced by the Dirichlet boundary condition at $z = z_0$. Fig. 3 illustrates how the terms of the sum in Eq. 3 contribute to construct the full response as $m$ increases. Notably, the first pair ($m \in [0, M-1]$ with $M = 2$) is sufficient to estimate the $\Delta T_{max}$ within 3% accuracy, while higher-order terms ($m{>}1$) only extend the steady state $\Delta T$ to longer times. By computing $\partial(\Delta T(z,t))/\partial t = 0$ with Eq. 3 truncated at $m = M - 1 = 1$, we analytically derive the 97% rise time as:

$$t_{r,97\%}(z) = t_{max}(z) = \frac{c_v z_0^2}{\kappa}\beta(z) = \tau_D \beta(z) \tag{4}$$

where $\tau_D = c_v z_0^2/k$, while $\beta(z)$ and $t_{max}(z)$ are the weak analytical functions of position shown in Fig. 4.

Two additional, distinct but equivalent expressions for $\Delta T(z,t)$ are obtained by inverse Laplace transform of Eq. 2 [10], which provides the system impulse response, and then integrating in time to obtain the step response as:

$$\Delta T(z,t) = P\left[\frac{z_0 - z}{A_0\kappa} - \sum_{n=0}^{\infty} R_n(z)\exp\left(-\frac{t}{\tau_n}\right)\right] \tag{5}$$

$$= P\sum_{n=0}^{\infty} R_n(z)\left[1 - \exp\left(-\frac{t}{\tau_n}\right)\right] \tag{6}$$

$$R_n(z) = \frac{8z_0}{A_0\pi^2\kappa}\frac{(-1)^n}{(2n+1)^2}\sin\left(\frac{(2n+1)\pi}{2z_0}(z_0 - z)\right) \tag{7}$$

$$\tau_n = \frac{4c_v z_0^2}{(2n+1)^2\pi^2\kappa} \quad . \tag{8}$$

In Eqs. 5, 6, $\Delta T(z,t)$ is expanded in an infinite spectrum of exponential terms each featuring *well-defined* thermal resistances, $R_n(z)$, and time constants, $\tau_n$, as per Eqs. 7, 8 and Fig. 5. Eq. 5 highlights the $z$-dependent steady state solution, whereas Eq. 6 allows us to interpret the step power response as due to a Foster network, as discussed in Sect. IV.

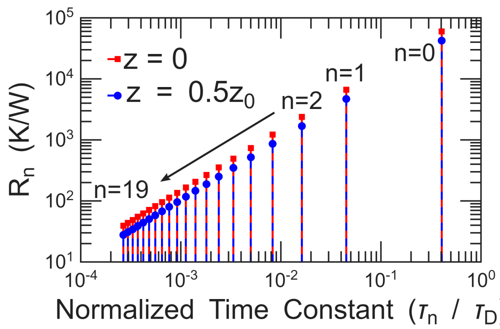


Fig. 5. Normalized time constants $\tau_n/\tau_D$ and thermal resistances $R_n(z)$ (Eqs. 7, 8 up to $N$=20) necessary to represent $\Delta T(z,t)$ at the source, $z = 0$, and at $z = z_0/2$. Parameters as in Fig. 2. $\tau_D = c_v z_0^2/\kappa$. Note that $R_n \propto \tau_n$ since they both scale as $(2n+1)^2$.

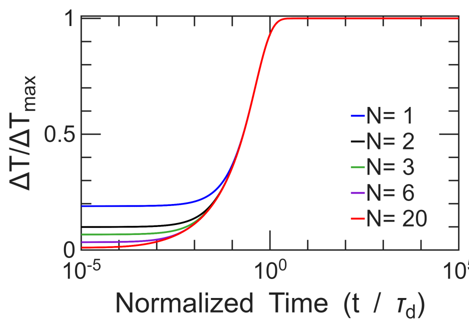


Fig. 6. Normalized $\Delta T(0,t)$ adding the terms with $n \in [0, N\text{-}1]$ in Eq. 5.

Fig. 6 shows how the addition of exponentials in Eq. 5, up to order $N$, leads the $\Delta T(z,t)$ waveforms to converge to the solution. Compared to Fig. 3, where the low-order terms accurately capture the initial transient, here they nicely reproduce the rising edge and the steady state, while the additional ones provide accuracy improvements only on the short timescale.

While Eqs. 3, 5, and 6 are perfectly equivalent, their truncation to a finite number of terms generates differences among them. The choice should thus be driven by considerations of computational efficiency and precision in predicting the transients and extracting physically meaningful $\kappa$ and $c_v$ values, as discussed in Sections III and IV, respectively.

## III. Efficient Estimation of Transients

Figs. 3, 6 suggest to search for the smallest $M$ and $N$ indexes ensuring that Eqs. 3, 5 are precise up (down) to given $t_h$ ($t_l$) values, respectively.

To this end, firstly, we consider the terms limiting the accuracy of Eq. 3 for long times, i.e. the $\mathrm{erfc}(\cdot)$ terms that contain $d_+$. These terms give contributions $\leq 16\%$ of their maximum value when $[2mz_0 - z]/[2\sqrt{\alpha t}] = 1$, a condition that strictly bounds the global truncation error to $\leq 3\%$ for $M > 2$. Therefore, the smallest integer $M$ that satisfies this condition up to $t_h$ is obtained by ceiling $\sqrt{\alpha t_h}/z_0 + z/2z_0$ but, since the terms should be taken in pairs to reproduce the correct $\Delta T_{max}$, the number of terms is:

$$M = 2\left\lceil \frac{\sqrt{\alpha t_h}}{z_0} + \frac{z}{2z_0} \right\rceil = 2\left\lceil \sqrt{\frac{t_h}{\tau_D}} + \frac{z}{2z_0} \right\rceil \quad . \tag{9}$$

As regards Eq. 5, the smallest $N$ ensuring less than $1\%$ error down to $t_l$, independent of $z$, is found by maximizing the $\sin(\cdot)$ function to 1, then enforcing $t_l/\tau_D = 5$ in the exponential, and ceiling the result to the adjacent integer. This yields:

$$N = \left\lceil \frac{\sqrt{5}z_0}{\pi\sqrt{\alpha t_l}} - 0.5 \right\rceil = \left\lceil \frac{\sqrt{5}}{\pi}\sqrt{\frac{\tau_D}{t_l}} - 0.5 \right\rceil \quad . \tag{10}$$

Eqs. 9, 10 provide the minimum number of terms to use in Eqs. 3, 5 to accurately calculate $\Delta T(z, t)$ up to $t_h$ and down to $t_l$, respectively. Fig. 7 reports their predictions and can be readily used to select the $M$ and $N$ that minimize the computation effort of Eqs. 3, 5 for given $t_l$ and $t_h$, respectively.

In addition, an accurate and efficient piecewise description of the whole temperature transient can be obtained selecting $M$=2, $N$=1, truncating the expressions at an appropriate $t^*$, and then retaining Eq. 3 for $t < t^*$ and Eq. 5 for $t > t^*$. Fig. 8 exemplifies this approach for $t^*$=0.5$\tau_D$, but any $t^*/\tau_D$ up to $\simeq$1 would yield similar results since Eq. 3 for $M$=2 and Eq. 5 for $N$=1 differ by less than 0.2% in this time interval.

## IV. Extraction of Physical Model Parameters

Let us now focus on the extraction of the physical parameters $\kappa$ and $c_v$ from the waveforms of thermal transients. Tab. I (first three lines) shows that the $\kappa$ and $c_v$ values extracted by fitting Eq. 3, and Eqs. 5, 7, 8 (truncated to the number of terms suggested by Eqs. 9, 10) to the TCAD temperature transient in Fig. 9 (where a white Gaussian noise with $\sigma$=1% $\Delta T_{max}$ has been added to mimic realistic experimental datasets) are in excellent agreement with the ones used in the TCAD,

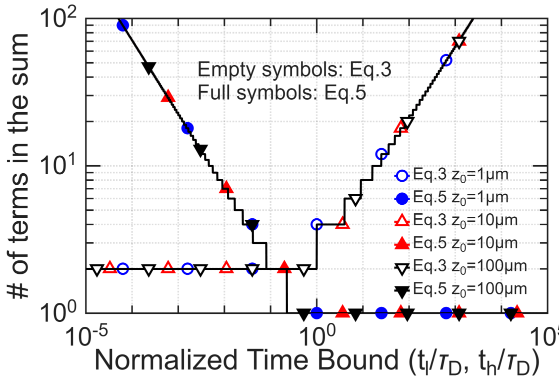


Fig. 7. Values of $M$ and $N$ to truncate Eqs. 3 and 5 computed with Eqs. 9 and 10 as a function of the chosen $t_h$ and $t_l$, respectively.

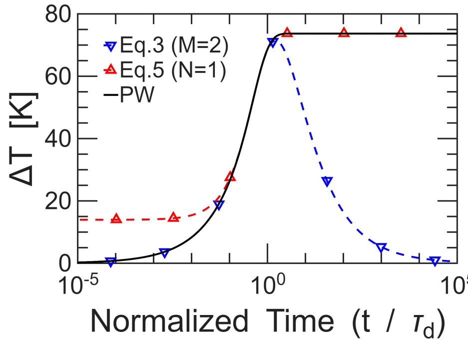


Fig. 8. Solid line: piecewise (PW) representation of $\Delta T(0, t)$ featuring the minimum number of terms, and obtained connecting Eq.3 for $M = 2$ with Eq. 5 for $N = 1$ at $t^* = 0.5\tau_D = 4.8$ ns where $\tau_D = 9.61$ ns.

thus confirming the validity of the proposed expressions and truncation method.

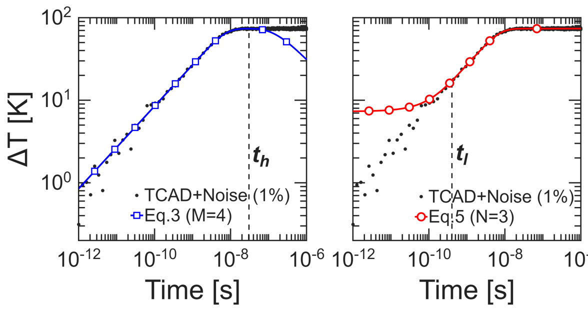


Fig. 9. Fitting of the truncated Eq. 3 (left, $M$=4) and Eq. 5 (right, $N$=3) to extract $\kappa$ and $c_v$ (values in Tab. I, first three lines). $t_l = 4 \cdot 10^{-10}$, $t_h = 3 \cdot 10^{-8}$. An AWG noise with $\sigma$=1%$\Delta T_{max}$ is added to the TCAD data to mimic realistic measurement conditions.

We also notice that Eq. 6 is equivalent to Eq. 5 but amenable to being represented as a Foster network of parallel $R_k$ and $C_k = \tau_k/R_k$ lumped elements (Fig. 10, top). These networks are commonly used to model the temperature dynamics of many devices, with typically one cell per decade of time [6], [12]. Their physical parameters are most often determined by

TABLE I

COMPARISON BETWEEN THE $\kappa$ AND $c_v$ USED IN THE REFERENCE TCAD SIMULATIONS AND THE ONES EXTRACTED BY FITTING DIFFERENTLY CONSTRAINED EXPRESSIONS TO THE TCAD (WITH ADDED NOISE AS IN FIG. 9) IN THE TIME INTERVAL $10^{-12} - 10^{-6}$s.

| **Method** | $\kappa$ (W/Kcm) | $c_v$ (J/Kcm$^3$) |
|---|---|---|
| 1) TCAD (reference) | 1.6964 | 1.63 |
| 2) Eq. 3, $M$=4, (Fig. 9) | 1.6945 | 1.61 |
| 3) Eqs. 5, 7, 8, $N$=3 (Fig. 9) | 1.6975 | 1.67 |
| 4) Eq. 6 & $R_{TOT}$, $N$=3, (Fig. 10) | 1.6964 | 8.79 |
| 5) Eqs. 6, 7, 8, 11, $N$=3, (Fig. 10) | 1.6966 | 1.61 |

fitting temperature transients, but the quality of the fit can be modest, and the extracted $R_k$ and $C_k$ (hence, $\kappa$ and $c_v$) are nonphysical [12]. These well-known issues are mitigated if the fit of the Foster network is constrained by imposing $R_{TOT} = \Delta T_{max}/P$ (see Fig. 10) to enforce matching the steady state hot spot temperature and so the correct $\kappa$ value. However, as demonstrated by the blue curve in Fig. 10 and the $4^{th}$ line in Tab. I, the quality of the fit to (noisy) TCAD is limited to a small time interval, and remarkably erroneous $c_v$ values are obtained, as expected. A significant improvement, however, is achieved using the truncated Eq. 6 if $R_N$ and $\tau_N$ are forced to take the values

$$R_N = \sum_{n=N}^{\infty} R_n \ ; \ \tau_N = \frac{\sum_{n=N}^{\infty} \tau_n R_n}{\sum_{n=N}^{\infty} R_n} \ ; \ C_N = \frac{\tau_N}{R_N} \quad (11)$$

while all the other $R_k$ and $\tau_k$ are as in Eqs. 7, 8. Indeed, the red curve in Fig. 10 shows that, by following this strategy, $\Delta T$ is in good agreement with the TCAD data over a much wider time interval, and the extracted $\kappa$ and $c_v$ are physically meaningful ($5^{th}$ line in Tab. I) in spite of the Foster circuit topology used.

## V. CONCLUSIONS

Three general expressions of $\Delta T(z,t)$ (Eqs. 3, 5, 6), and their truncated but accurate forms, have been derived for an ideal stepwise power source. A simple expression for the rise time (Eq. 4), and criteria to maximize the $\Delta T(z,t)$ computation efficiency for a given time interval have been provided as well (Fig. 7). The equations can be used to predict the self-heating (i.e., the temperature at the power source, $z$=0) and cross-heating (i.e., the temperature at the location of a victim device, $z\neq 0$) contributions to the overtemperature, to optimize the source-victim distance, and to extract physically meaningful thermal parameters, thus overcoming some limitations of commonly adopted Foster networks. To this end, we found critical to respect the constraints set by Eqs. 7, 8 during the fitting process. In practical situations where the measurement time step and/or the power source rise/fall times are finite ($t_{s,r,f}$), we expect the formulas to remain accurate only for $t \gtrsim t_{s,r,f}$; this may lead to prefer using Eqs. 5 to Eq. 3, due to the faster convergence for large times.

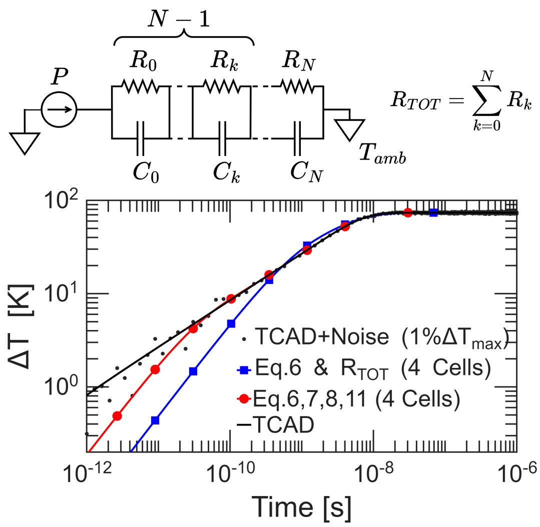


Fig. 10. Top: Schematic of a Foster-type equivalent thermal circuit. Bottom: $\Delta T(0,t)$ from TCAD with added noise (black line with dots) and corresponding curves for a 4 cells Foster network. Blue: fitted imposing $R_{TOT} = \Delta T_{max}/P$. Red: fitted imposing Eqs. 7, 8 to the first $N-1$ cells and Eq. 11 to the $N$-th cell. Parameters as in Fig. 2.

## REFERENCES


[1] H. Jiang et al., "FEOL Self-heating and BEOL Joule-heating Effects of FinFET Technology and Its Implications for Reliability Prediction," 2020 IEEE International Integrated Reliability Workshop (IIRW), South Lake Tahoe, CA, USA, 2020, pp. 1-5, doi: 10.1109/IIRW49815.2020.9312859.

[2] E. Bury et al., "Self-heating in FinFET and GAA-NW using Si, Ge and III/V channels," 2016 IEEE International Electron Devices Meeting (IEDM), San Francisco, CA, USA, 2016, pp. 15.6.1-15.6.4, doi: 10.1109/IEDM.2016.7838425.

[3] D. Jang, S. -G. Jung, S. -J. Min and H. -Y. Yu, "Electrothermal Characterization and Optimization of Monolithic 3D Complementary FET (CFET)," in IEEE Access, vol. 9, pp. 158116-158121, 2021, doi: 10.1109/ACCESS.2021.3130654.

[4] S. E. Liu et al., "Self-heating effect in FinFETs and its impact on devices reliability characterization," 2014 IEEE International Reliability Physics Symposium, Waikoloa, HI, USA, 2014, pp. 4A.4.1-4A.4.4, doi: 10.1109/IRPS.2014.6860642.

[5] K. R. Bagnall and E. N. Wang, "Theory of Thermal Time Constants in GaN High-Electron-Mobility Transistors," in IEEE Trans. on Components, Packaging and Manufacturing Technology, vol. 8, no. 4, pp. 606-620, April 2018, doi: 10.1109/TCPMT.2017.2773065.

[6] A. Weyman, "A Guide to Improving Thermal Simulations With Refined Foster and Cauer Models," in IEEE Power Electronics Magazine, vol. 12, no. 4, pp. 75-83, Dec. 2025, doi: 10.1109/MPEL.2025.3583278.

[7] H. S. Carslaw and J. C. Jaeger, Conduction of Heat in Solids, 2nd ed. Oxford, U.K.: Clarendon Press, 1959.

[8] M. S. Ghausi and J. J. Kelly, Introduction to Distributed-Parameter Networks: With Application to Integrated Circuits. New York, NY, USA: Holt, Rinehart and Winston, 1968.

[9] R. E. Matick, Transmission Lines for Digital and Communication Networks. New York, NY, USA: IEEE Press, 1995.

[10] M. Abramowitz and I. A. Stegun, *Handbook of Mathematical Functions with Formulas, Graphs, and Mathematical Tables*, National Bureau of Standards Applied Mathematics Series, vol. 55. Washington, DC, USA: U.S. Government Printing Office, 1964.

[11] Synopsys, Inc., Raphael™ FX User Guide, Synopsys manual.

[12] K. Ma, N. He, M. Liserre and F. Blaabjerg, "Frequency-Domain Thermal Modeling and Characterization of Power Semiconductor Devices," in IEEE Trans. on Power Electronics, vol. 31, no. 10, pp. 7183-7193, Oct. 2016, doi: 10.1109/TPEL.2015.2509506.